International Journal of Fluid Machinery and Systems
Vol. 3, No. 1, January-March 2010

Original Paper

Measurements of Minute Unsteady Pressure on Three-Dimensional Fan with Arbitrary Axis Direction

Katsuya Hirata[1], Takuya Fuchi[1], Yusuke Onishi[1], Akira Takushima[2], Seiji Sato[2] and Jiro Funaki[1]

[1]Department of Mechanical Engineering, Doshisha University
Kyoto 610-0321, Japan
[2]Samsung Yokohama Research Institute
Minoo 562-0036, Japan

Abstract

The present study is a fundamental approach to develop the measuring technology for minute fluctuating pressures on the three-dimensional blade surfaces of the fan which rotates with an arbitrary rotation-axis direction. In this situation, we are required to correct the centrifugal-force effect, the gravitational-force effect and the other leading-error effects for accurate measurements of the minute pressures. The working fluid is air. A pressure transducer rotating with an arbitrary attitude is closely sealed by a twofold shroud system. The rotational motion with an arbitrary attitude is produced by fixing the pressure transducer to the cantilever which is connected to a motor-driven disc of 500mm in diameter and 5mm in thickness. As a result, we have quantitatively determined main governing effects upon the non-effective component of the pressure-transducer signal.

Keywords: Fluctuating pressure, Pressure measurement, Unsteady pressure, Fan, Low speed.

1. Introduction

We often find various kinds of fans in many industrial equipments and home electric appliances like ventilation, mixing and cooling devices. Recently, according to the requirements for low sound-noise level, for high performance and for high efficiency, researchers have been tackling dramatic innovations using three-dimensional fan designs and using sophisticated analytical techniques in experiments and computations.

In spite of many past researches, the flows around fans have not been clear yet, because of the inherent complexity of the flows with three dimensionality, with non-linearity and with the moving boundaries related to rotating blades at high Reynolds numbers. While numerical approaches have been becoming powerful tools in the recent development of computer resources, we can not estimate their accuracies yet without accompanying experimental studies. In this context, the accurate experimental results can be also dedicated to Computational Fluid Dynamics (know as CFD) as a standard benchmark.

Among the concerning physical quantities, the unsteady pressures on the rotating blades give us useful information for the fan flow and its sound-noise level. However, there have been only several accurate works (Zheng et al., 1996 [1]; Huyer et al., 1996 [2]; Carolus & Stremel; 2002 [3]) due to technical difficulties such as (1) much smaller pressure-fluctuation amplitudes of fans than blowers and compressors, (2) blade rotations and (3) three dimensionalities of blades' geometries. For high-speed fans with large pressure-fluctuation amplitudes, these difficulties could reduce (for example, see Xu & Amano, 2002 [4]). Recently, we have conducted the unsteady-pressure measurements but for a very simple model under restricted experimental conditions, where the rotation axis is parallel to the gravity direction, and where the fan is two-dimensional (Hirata et al., 2008 [5]).

The present study is a fundamental approach to develop the measuring technology for minute fluctuating pressures on three-dimensional blade surfaces of the fan with an arbitrary rotation-axis direction, where we are required to correct the centrifugal-force effect, the gravitational-force effect and the other leading-error effects for accurate measurements. We expect that the precise pressures measured by the present technology will contribute to fan-design innovations.

2. Experimental Method

Figure 1 shows the present experimental apparatus for the measurement of non-effective component p_{ne} of pressure-transducer signal. The working fluid is air. A model is a pressure transducer in a rotational motion with an arbitrary attitude, which is closely sealed by a twofold shroud system, that is to say, shrouds A and B. The dimensions of the transducer are 10mm in diameter and 3mm in thickness, and see Ref. [5] in detail. A disc, whose dimensions are 500mm in diameter and 5mm in

Received October 14 2009; revised November 9 2009; accepted for publication November 16 2009: Review conducted by Prof. Wu Yulin. (Paper number O09047)
Corresponding author: Katsuya Hirata, Professor, khirata@mail.doshisha.ac.jp

thickness, is driven by an outside electric motor via a driving shaft, with a constant rotation speed N. Its rotation axis is horizontal, and its rotational direction is anti-clockwise.

The signal from the transducer is transmitted to an outside PC with an A/D-converter board via a telemeter. In the present study, the telemeter is necessary to detect minute pressure signals, being free from the noises synchronised with the disc rotation. Because, the synchronised noises are inevitable in conventional slip rings.

Besides, in order to diminish mechanical vibrations related with the disc rotation, we place the telemeter and its battery on the opposite of the cantilever, together with an appropriate counter weight.

Concretely speaking, the transducer is fixed on a cantilever. The cantilever is connected to the rotating disc with variable angles ϕ and ψ (for their definitions, see Fig. 2), at some values of the radial distance r from the origin, the disc-rotation centre. Then, ϕ and ψ correspond to the two inclination angles of the transducer in order to specify the transducer's attitude.

In summary, we consider such four control parameters as r, N, ϕ and ψ. If we can estimate the individual effects of those control parameters upon the transducer signal under the condition that the rotation axis is not vertical, we can accurately correct the signal from the transducer on the fan blade with an arbitrary rotation-axis direction and with an arbitrary attitude.

In addition, to confirm the validity of the present measuring technology, we finally carry out the direct measurement of the blade-surface pressure of a propeller fan. Figure 3 shows an experimental apparatus for the measurement of pressure on a propeller fan. A pressure transducer is flush-mounted on the pressure surface (namely, the pressure side of the blade surfaces) of the fan. Then, the diaphragm of the pressure transducer is on the same level as the blade surface. A measuring position, that is, the position of the pressure-transducer centre is at r = 155mm on the centre of a blade with a setting angle of $\pi/6$. The fan's dimensions are 235mm in fan radius, 5mm in blade thickness and 73mm in hub radius. The fan is covered by an annular casing of 290mm in length and 10mm in thickness.

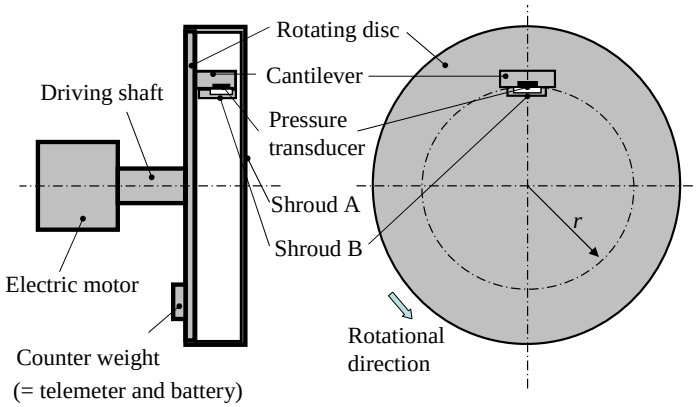

Fig. 1 Experimental apparatus for the measurement of non-effective component p_{ne} of pressure-transducer signal.

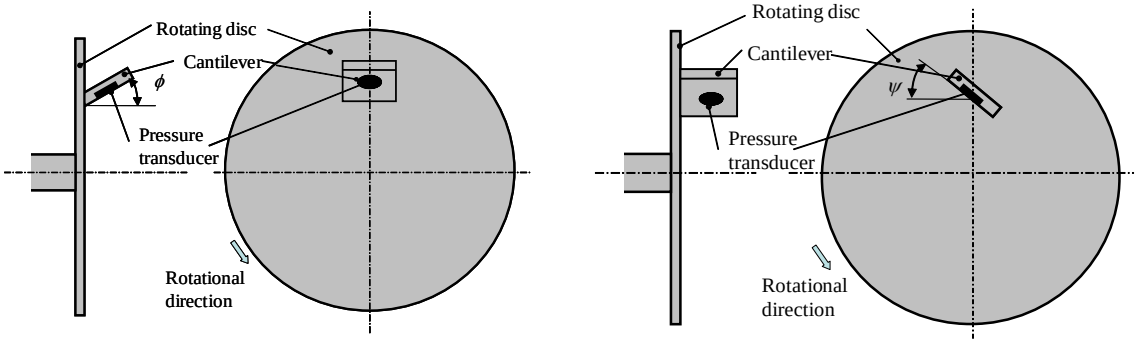

(a) ϕ (b) ψ

Fig. 2 Definitions of pressure-transducer inclination angles ϕ and ψ.

3. Results and Discussion

3.1 Pressure-Transducer Signal p_{ne}

In general, the signal p out of a pressure transducer involves not only an effective surface-pressure component p_e, but also a non-effective component p_{ne} which is unrelated to actual surface pressure. In the present study, we try to estimate p_{ne}, quantitatively. Then, we closely seal the transducer by the twofold shroud system, in order to make p_e approximately zero.

Figure 4 shows a sample time history of pressure-transducer signal p_{ne} (shown as a black line in the figure), together with (1) its running-averaged value p_{ne}^* (shown as a light-gray line in the figure) which is a subtractor from the raw data p_{ne} by higher-frequency random noises, and (2) its time-mean value $\overline{p}_{ne}$ (shown as a dotted line in the figure). Here, superscripts '*' and '¯' denote running-averaged and time-mean, respectively.

In the present study, we deal with only the running-averaged value instead of raw signal, in order to diminish randomly-fluctuating components with high frequencies. Although the running-average technique is useful in practical aspects in actual measurements, some considerations are needed to consider raw data correctly.

We divide p_{ne} into three components as follows.

$$p_{ne} = \overline{p}_{ne} + \tilde{p}_{ne} + \hat{p}_{ne} \quad . \tag{1}$$

Superscripts '~' and 'ˆ' denote periodically-fluctuating and randomly-fluctuating, respectively. Then, the running-averaged signal is

$$p_{ne}^{\ *} = \overline{p}_{ne}^{\ *} + \tilde{p}_{ne}^{\ *} + \hat{p}_{ne}^{\ *} \quad , \tag{2}$$

where

$$\overline{p}_{ne}^{\ *} = \overline{p}_{ne} \quad . \tag{3}$$

In Fig. 4, we can confirm that p_{ne}^* approximately consists of two components $\overline{p}_{ne}$ and $\tilde{p}_{ne}^{\ *}$. If a raw signal is sinusoidal, we can guess it using the correction factor F for the running-averaged signal. F is defined by

$$(\tilde{p}_{ne})_{amp} = (\tilde{p}_{ne}^{\ *})_{amp} / F \tag{4}$$

with

$$F = \frac{\sin(\pi N \tau)}{\pi N \tau} \quad , \tag{5}$$

where a subscript 'amp' and τ denote amplitude and running-average period, respectively. In the present study, as the magnitude of $\hat{p}_{ne}$ is in low level and as the dominant frequencies of $\hat{p}_{ne}$ is very high, such a small τ as $0.03/N$ is enough for smoothing, where F = 0.998 according to Eq. (5). Then, we hereafter regard $\tilde{p}_{ne}^{\ *}$ as $\tilde{p}_{ne}$, because $\tilde{p}_{ne}^{\ *} \approx \tilde{p}_{ne}$. In the following subsections, we will consider only both the components $\overline{p}_{ne}$ and $\tilde{p}_{ne}$.

3.2 Time-Mean Component $\overline{p}_{ne}$

Figure 5 shows the time-mean component $\overline{p}_{ne}$ of the pressure-transducer signal at ϕ = 0 and ψ = 0, plotted against the rotation speed N, for some values of the radial location r of the transducer. We can see that $\overline{p}_{ne}$ monotoneously increases with increasing N, and that $\overline{p}_{ne}$ monotoneously increases with increasing r. In the figure, error bars denote the maximum and the minimum values during the averaging time of 180sec, to specify the uncertainty of the present measurements.

If $\overline{p}_{ne}$ is almost governed by the centrifugal force of such masses as pressure-transducer diaphragm mass, ambient fluid mass and so on, $\overline{p}_{ne}$ is in proportion to N^2, and in proportion to r.

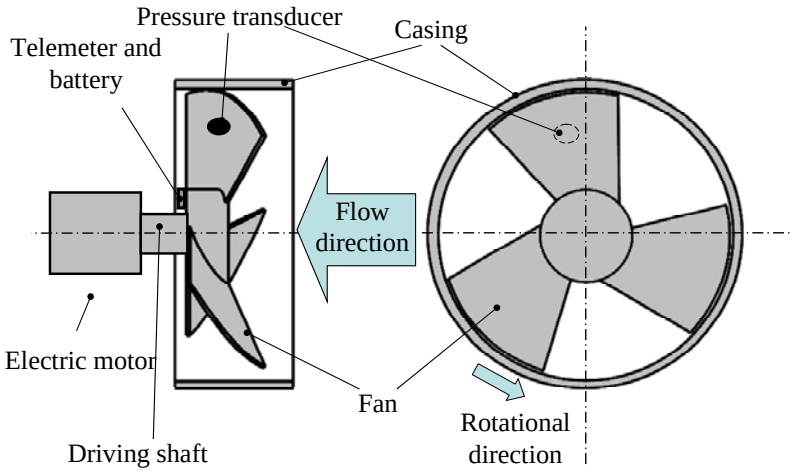

Fig. 3 Experimental apparatus for the surface-pressure measurement on a propeller fan. A pressure transducer is fixed on a pressure surface (that is, the pressure side of a blade surface) of the fan.

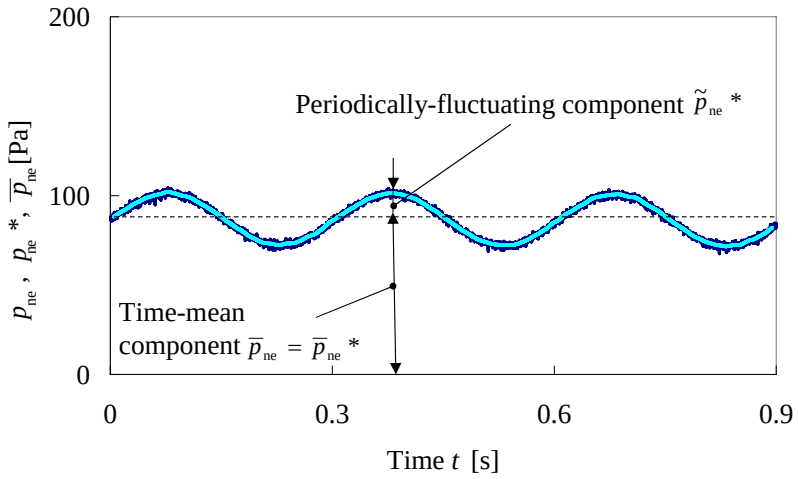

Fig. 4 Time histories of pressure-transducer signals at r = 130mm, N = 3.3Hz, ϕ = 0 and ψ = 0. A black line, raw data p_{ne}; a light-gray line, running-averaged value p_{ne}* with an averaging period τ = 0.01s; a dotted line, time-mean value $\overline{p}_{ne}$.

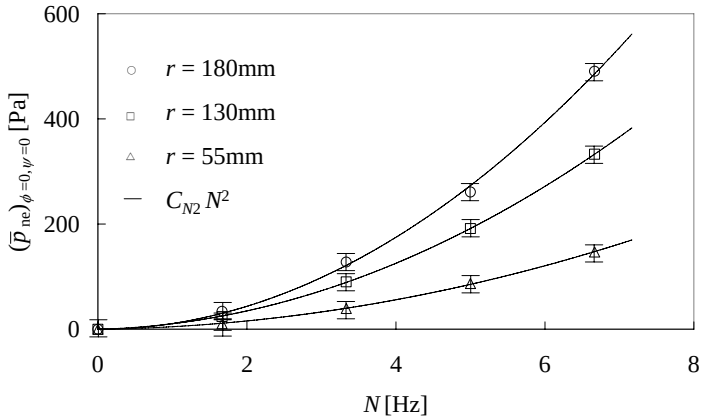

Fig. 5 Time-mean component $\overline{p}_{ne}$ of the pressure-transducer signal at ϕ = 0 and ψ = 0, against rotation speed N. Error bars denote the maximum and the minimum values during the averaging time of 180sec.

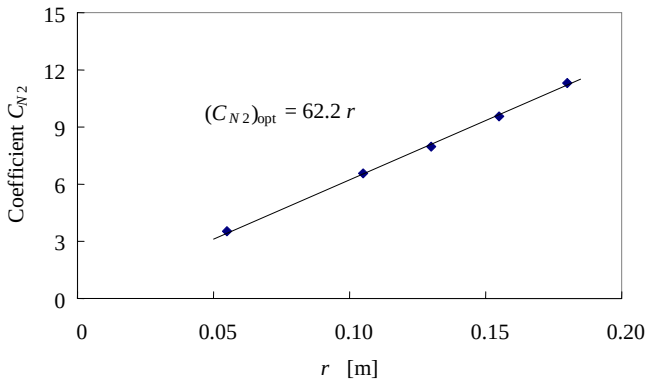

Fig. 6 Coefficient C_{N2} against the radial location r of a pressure transducer. Each plot of C_{N2} is calculated by the least-square a pproximation over N = 0 – 6.7Hz at ϕ = 0 and ψ = 0.

Three solid curves in the figure represent the least-square approximations over N = 0 – 6.7Hz at ϕ = 0 and ψ = 0, for three values of r. Here, we suppose such a relation as $\overline{p}_{\mathrm{ne}} \propto N^2$. As a result, we can confirm that

$$(\overline{p}_{\mathrm{ne}})_{\phi=0,\,\psi=0} \approx C_{N2} N^2, \tag{6}$$

where C_{N2} denotes a coefficient related with the masses, which depends upon r.

Furthermore, we can also confirm that C_{N2} is almost in proportion to r. Figure 6 shows five values of C_{N2} obtained using the least-square approximation, three of which are shown in Fig. 5, plotted against r. C_{N2} can be approximated in such an optimum straight line as

$$(C_{N2})_{\mathrm{opt}} = 62.2r \tag{7}$$

In summary, at ϕ = 0 and ψ = 0, we can now identify $\overline{p}_{\mathrm{ne}}$ as the centrifugal-force component p_{c}, because $\overline{p}_{\mathrm{ne}} \propto N^2$ and $\overline{p}_{\mathrm{ne}} \propto r$. If $\overline{p}_{\mathrm{ne}}$ at $\phi \neq 0$ or $\psi \neq 0$ is governed only by the centrifugal force as well, $\overline{p}_{\mathrm{ne}}$ with arbitrary values of r, N, ϕ and ψ is given by the following equation with $(C_{N2})_{\mathrm{opt}}$ in Eq. (7).

$$\overline{p}_{\mathrm{ne}} = p_{\mathrm{c}} = (C_{N2})_{\mathrm{opt}}\, N^2 \cos\phi \cos\psi. \tag{8}$$

In order to check the validity of Eq. (8) with Eq. (7), we show some examples. Figures 7, 8, 9 and 10 show $\overline{p}_{\mathrm{ne}}$ at ϕ = 0 and $\psi = \pi/6$, at ϕ = 0 and $\psi = \pi/3$, at $\phi = \pi/6$ and ψ = 0, and at $\phi = \pi/3$ and ψ = 0, respectively, which are plotted against N for two values of r. As a result, we can see that all data fairly collapse on two solid curves which represent Eq. (8) with Eq. (7).

3.3 Periodically-Fluctuating Component $\tilde{p}_{\mathrm{ne}}$

Figure 11 shows the static gravitational-force component p_{g} of the pressure-transducer signal plotted against the inclination angle θ of the pressure transducer from the horizontal plane. Specifically speaking, p_{g} is the time-mean signal from the transducer which is placed in stationary air with its diaphragm attitude of θ, as shown as an illustration in the figure. By such static experiments with no rotation, p_{g} can be approximated by the following relation.

$$p_{\mathrm{g}} = C_{\mathrm{g}} \cos\theta, \tag{9}$$

with

$$C_{\mathrm{g}} = 15.8. \tag{10}$$

The relation is drawn by a solid curve in the figure.

We have conducted many rotation experiments, and confirmed that those experiments agree well with Eq. (9) with Eq. (10). Table 1 shows some sample results, namely, periodically-fluctuating amplitude $(\tilde{p}_{\mathrm{ne}})_{\mathrm{amp}}$, together with amplitude $(p_{\mathrm{g}})_{\mathrm{amp}}$ of the static gravitational-force, for several values of N, ϕ and ψ. Note that, in rotation experiments, θ in Eq. (9) is replaced by ϕ. As a result, we can find that the fluctuating component of $\tilde{p}_{\mathrm{ne}}$ is almost coincides with p_{g} in various situations, which can be approximately given by

$$\tilde{p}_{\mathrm{ne}} = p_{\mathrm{g}} = C_{\mathrm{g}} \cos\phi \cos 2\pi N t. \tag{11}$$

with C_{g} in Eq. (10).

If we regard the diaphragm mass of the transducer as only one main factor of p_{ne}, we can suppose such a relation between the two coefficients $(C_{N2})_{\mathrm{opt}}$ and C_{g} as

$$(C_{N2})_{\mathrm{opt}} = 4\pi^2 r C_{\mathrm{g}} / g. \tag{12}$$

Of course, this relation is not rigorous in any case, due to neglected factors like the ambient fluid around the diaphragm, the diaphragm structure and so on. About the present transducer, the relative error for Eq. (12) is 1.9%. However, from another viewpoint, if we accept a relative error in such a level, we can predict $(C_{N2})_{\mathrm{opt}}$ from C_{g} using Eq. (12), and vice versa.

3.4 Pressure on a Propeller Fan

Finally, in order to confirm the validity of the measuring technology developed above, we conduct the measurement for an actual propeller fan, as shown in Fig. 3.

Figure 12(a) shows a time history of a raw pressure-transducer signal p on the pressure-surface centre of the propeller-fan blade at r = 155mm, N = 9.7Hz, $\phi = \pi/6$ and $\psi = \pi/2$, during 29.1 periods of fan's rotation. And, Fig. 12(b) shows its corresponding spectrum. In Fig. 12(a), the raw signal fluctuates with a dominant frequency of about 10Hz which is approximately equal to N, having higher-frequency components. In fact, we can see an distinguished spectral peak at $f = N$ in Fig. 12(b). Furthermore, we can see that the higher-frequency components mainly consist of two higher harmonics with $f = 4N$ and $f = 7N$. These two higher harmonics are considered to be related with structural resonances. By a preliminary experiment, we have clearly observed two structural eigen frequencies f_{s1} and f_{s2}, which are for the experimental-apparatus platform and for the fan, respectively. Two dashed lines in the figure denote $f = f_{\mathrm{s1}}$ and $f = f_{\mathrm{s2}}$. We can see that these are very close to $f = 4N$ and $f = 7N$.

Figure 13 shows time histories of pressure-transducer signal (raw data) p on the pressure-surface centre during one period of fan's rotation, together with the phase-averaged pressure p^{p} over 30 periods of fan's rotation, the effective phase-averaged pressure (corrected data) $p_{\mathrm{e}}{}^{\mathrm{p}} = p^{\mathrm{p}} - \tilde{p}_{\mathrm{ne}}$, and $\overline{p}_{\mathrm{e}} + \tilde{p}_{\mathrm{ne}}$. The abscissa is the rotation angle Θ of the propeller fan, instead of time t.

At first, when we compare p and p^{p}, we can confirm the combined contribution upon p of the non-periodical components

related with randomly-fluctuating turbulent flows and of the periodical components with non-harmonic frequencies related with mechanical vibrations and oscillatory instable flows. The contribution is pretty large. Next, when we compare p_e^p with p^p, we can see that p_e^p is corrected to be more independent of time t than p^p; that is, p_e^p is less periodical than p^p. This more independency of t suggest that the present measuring system is effective, as the more independency of t should be proper in this experiment. We can confirm the more independency of t more clearly, if we compare p_e^p with $\overline{p}_e + \widetilde{p}_{ne}$ instead of p^p. That is, $\overline{p}_e + \widetilde{p}_{ne}$ fluctuates at $f = N$ with a much larger amplitude than p_e^p.

Supplementarily speaking, when we compare p^p and $\overline{p}_e + \widetilde{p}_{ne}$, we can see that p^p fluctuates with higher frequencies than N. But p^p is always very close to $\overline{p}_e + \widetilde{p}_{ne}$. This suggests that $\widetilde{p}_e$ is small. Because $\psi = \pi/2$, $\overline{p}_{ne}$ is considered to be almost zero. In addition, the flow is considered to be almost steady in a frame of reference concerning the fan's blade. Then, it seems reasonable that $\widetilde{p}_e$ might be neglected.

Figure 14(a) shows a time history of the corrected pressure-transducer signal p_e^p during 29.1 periods of fan's rotation, instead of one period in Fig. 13. And, Fig. 14(b) shows its corresponding spectrum. In Fig. 14(a), we can see that p_e^p is almost constant being independent of t in comparison with p in Fig 12(a), although small amplitude and high-frequency fluctuations still remain. We can confirm this by the spectrum in Fig. 14(b), as well. Namely, the spectral peak at $f = N$ in Fig. 14(b) becomes much lower than that in Fig. 12(b). As well as the spectral peak at $f = N$, the spectral peaks at $f = 4N$ and $f = 7N$ in Fig. 14(b) become lower than those in Fig. 12(b), although they are still clear. In other words, such an error in the pressure-fluctuation magnitude of acquired data as less than 10Pa should be permitted in the present measuring system.

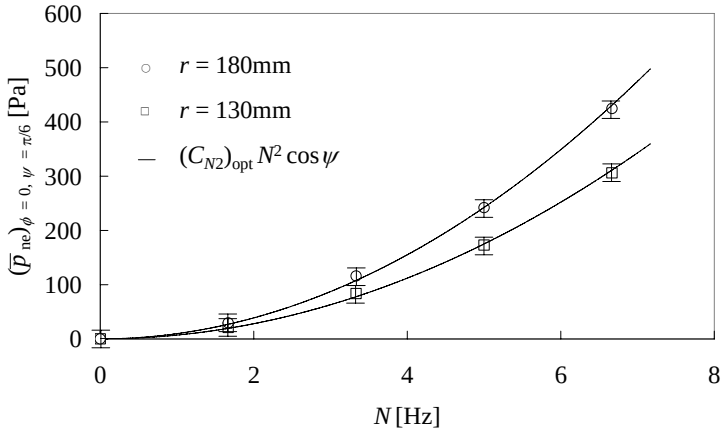

Fig. 7 Time-mean component $\overline{p}_{ne}$ of the pressure-transducer signal at $\phi = 0$ and $\psi = \pi/6$, against rotation speed N. Error bars denote the maximum and the minimum values during the averaging time of 180sec.

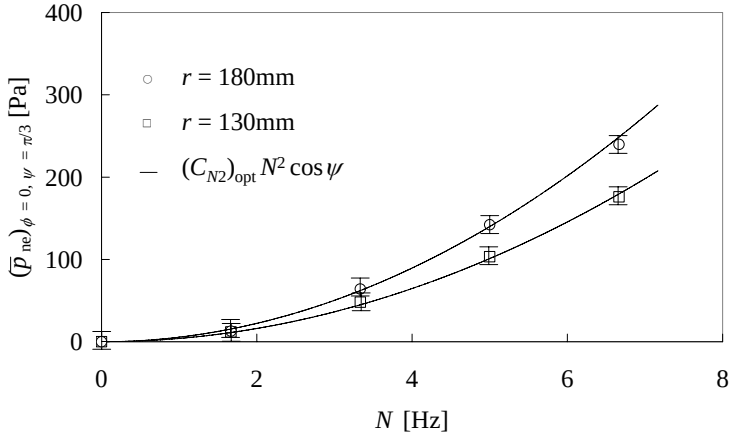

Fig. 8 Time-mean component $\overline{p}_{ne}$ of the pressure-transducer signal at $\phi = 0$ and $\psi = \pi/3$, against rotation speed N. Error bars denote the maximum and the minimum values during the averaging time of 180sec.

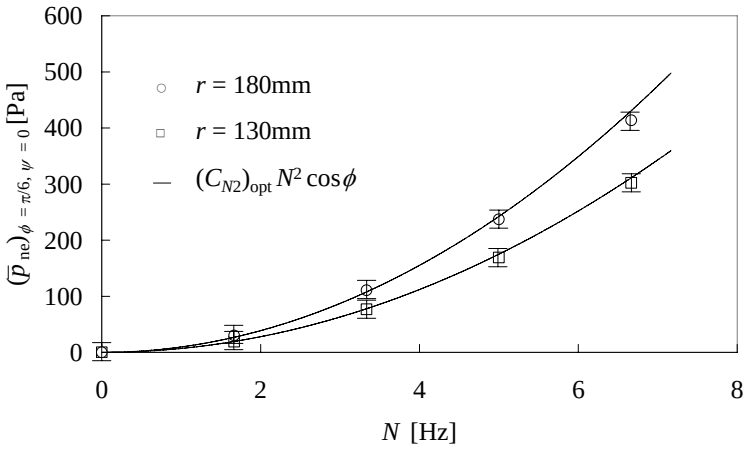

Fig. 9 Time-mean component $\overline{p}_{ne}$ of the pressure-transducer signal at $\phi = \pi/6$ and $\psi = 0$, against rotation speed N. Error bars denote the maximum and the minimum values during the averaging time of 180sec.

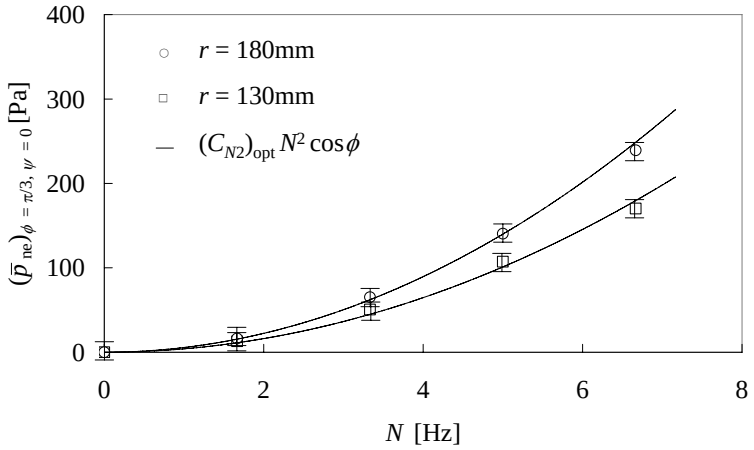

Fig. 10 Time-mean component $\overline{p}_{ne}$ of the pressure-transducer signal at $\phi = \pi/3$ and $\psi = 0$, against rotation speed N. Error bars denote the maximum and the minimum values during the averaging time of 180sec.

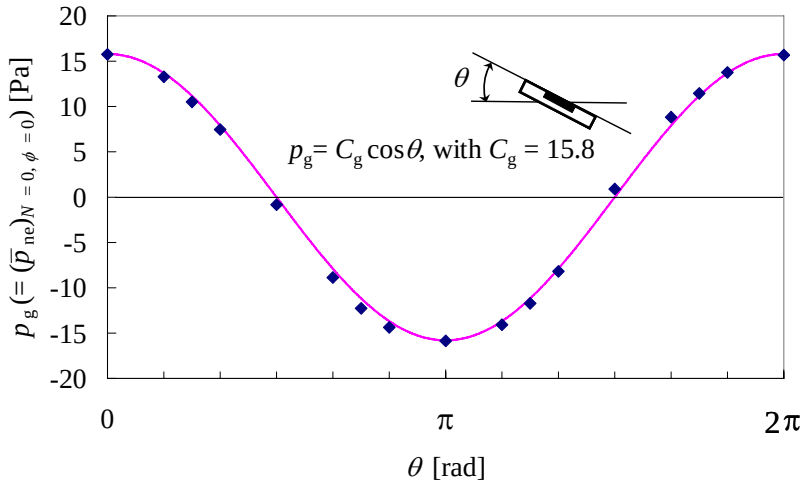

Fig. 11 Gravitational-force component p_g of pressure-transducer signal against inclination angle θ from the horizontal plane in stationary air.

Table 1 Periodically-fluctuating amplitude $(\tilde{p}_{ne})_{amp}$, together with amplitude $(p_g)_{amp}$ of static gravitational-force component.

$r\times10^{-3}$ [m]	N [rps]	ϕ [rad]	ψ [rad]	$(\tilde{p}_{ne})_{amp}$ [Pa] *1	$(p_g)_{amp} = 15.8\cos\phi$ [Pa]
130	1.67	0	0	16.1	15.8
130	6.67	0	0	15.7	15.8
130	1.67	π/6	0	14.0	13.7
130	6.67	π/6	0	15.2	13.7
130	1.67	π/3	0	8.3	7.9
130	6.67	π/3	0	8.4	7.9
130	1.67	0	π/6	15.6	15.8
130	6.67	0	π/6	15.8	15.8
130	1.67	0	π/3	15.3	15.8
130	6.67	0	π/3	14.8	15.8

＊1 Strictly speaking, $(\tilde{p}_{ne})_{amp}$ is a periodically-fluctuating amplitude $(\tilde{p}_{ne}{}^{*})_{amp}$ of pressure transducer signal with a running-average period $\tau = 0.03/N$.

4. Conclusions

In order to develop the measuring technology for minute fluctuating pressures on the three-dimensional blade surfaces of the fan which rotates with an arbitrary rotation-axis direction, we have successfully estimated leading effects on the non-effective component p_{ne} of the pressure-transducer signal, quantitatively. In the present measuring system, we can conclude that p_{ne} approximately consists of only two; namely, a centrifugal-force component p_c and a gravitational-force component p_g. Finally, to confirm the validity of the present measuring technique, we have carried out the direct measurement of the blade-surface pressure of a propeller fan.

Acknowledgement

We appreciate technical support by Mr Shigeya Nagasaka (Doshisha University).

Nomenclature

C_{N2}	Coefficient related with masses
D	Diameter [mm]
F	Correction factor for running averaging
N	Rotation speed [Hz]
p	Pressure [Pa]
r	Radial distance [mm]
t	Time [s]
τ	Running-average period [s]
Θ	Rotation angle of fan [rad]
θ, ϕ, ψ	Inclination angle [rad]

Superscripts

~	Periodically-fluctuating
*	Running-averaged
^	Randomly-fluctuating
‾	Time-mean
p	Phase-averaged

Subscripts

amp	Amplitude
c	Centrifugal-force
e	Effective
g	Gravitational-force
ne	Non-effective
opt	Optimum

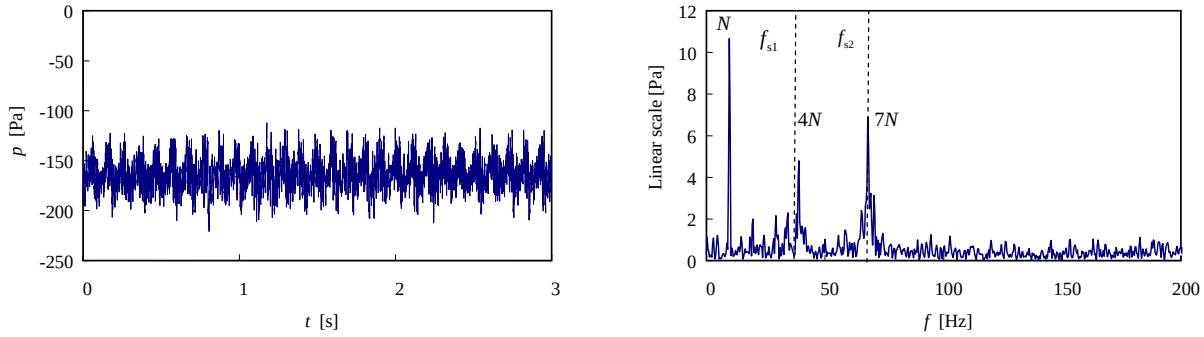

(a) Time history (b) Spectrum

Fig. 12 Time history and spectrum of pressure-transducer signal (raw data) p on the pressure-surface centre at r = 155mm, N = 9.7Hz, $\phi = \pi/6$ and $\psi = \pi/2$.

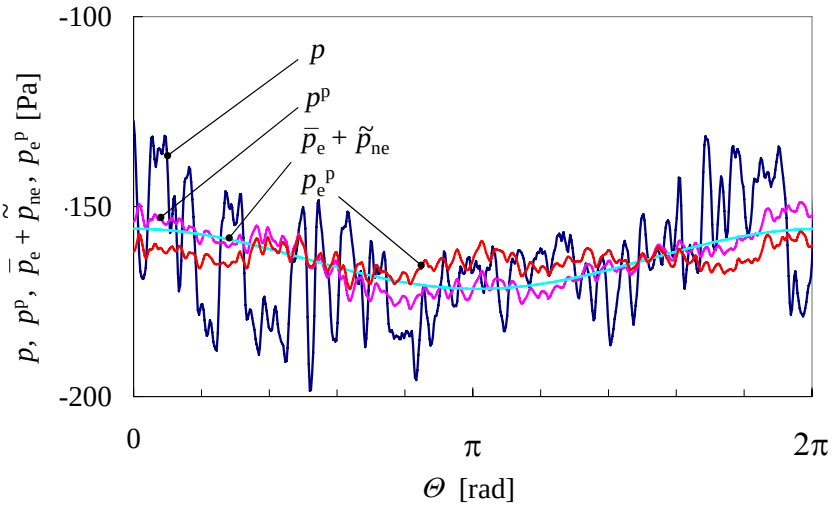

Fig. 13 Time histories of pressure-transducer signal (raw data) p on the pressure-surface centre at r = 155mm, N = 9.7Hz, $\phi = \pi/6$ and $\psi = \pi/2$ during one period, together with the phase-average pressure p^{p} over 30 periods, the effective phase-average pressure (corrected data) $p_e^{p} = p^{p} - \tilde{p}_{ne}$, and $\bar{p}_e + \tilde{p}_{ne}$.

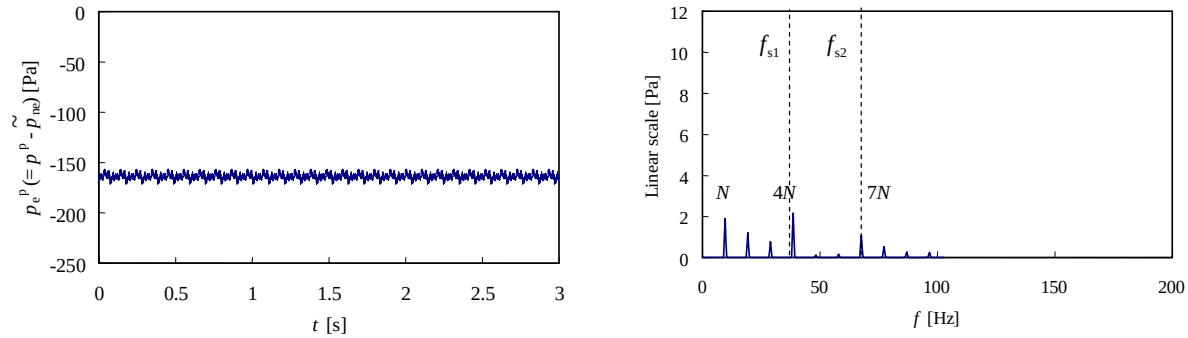

(a) Time history (b) Spectrum

Fig. 14 Time history and spectrum of corrected pressure-transducer signal p_e^{p} on the pressure-surface centre at r = 155mm, N = 9.7Hz, $\phi = \pi/6$ and $\psi = \pi/2$.

References

[1] Z. Zheng, S. Sato and K. Kinoshita, 1996, “Experimental Study on Low Noise Propeller Fan,” Proc. Fluids Engineering Division Conf., ASME, FED-Vol. 237, Vol. 2, pp. 61-65.
[2] S. A. Huyer, D. Simmis and M. Robinson, 1996, “Unsteady Aerodynamics Associated with a Horizontal-Axis Wind Turbine,” AIAA Journal, Vol. 34, No. 7, pp. 1410-1419.
[3] T. H. Carolus and M. Stremel, 2002, “Blade Surface Pressure Fluctuations and Acoustic Radiation from an Axial Fan Rotor due to Turbulent Flow,” Acta Acustica united with Acustica, Vol. 88, pp. 472-482.
[4] C. Xu and R. S. Amano, 2002, “Unsteady Pressure Field Investigation of an Axial Fan –Blade Unsteady Pressure Field Measurement–,” International Journal of Rotating Machinery, Vol. 8, No. 6, pp. 385-395.
[5] K. Hirata, Y. Iida, A. Takushima and J. Funaki, 2008, “Instantauous Pressure Measurement on a Rotating Blade of Cross-Flow Impeller,” JSME J. Environment and Engineering, Vol. 3, No. 2, pp. 261-271.